P13.16 DROP SHAPE STUDIES IN RAIN USING 2-D VIDEO DISDROMETER AND DUAL-WAVELENGTH, POLARIMETRIC CP2 RADAR MEASUREMENTS IN SOUTH-EAST QUEENSLAND, AUSTRALIA

M. Thurai[1*], V. N. Bringi[1], and P. T. May[2]

[1]Colorado State University, Fort Collins, Colorado, USA
[2]Centre for Australian Weather and Climate Research, Australia

1. INTRODUCTION

The shape of rain drops has been studied in various ways over the past several decades, amongst them being (i) wind-tunnel measurements by Pruppacher and Beard (1970), (ii) numerical modelling of equilibrium drop shapes by Beard and Chuang (1987) and (iii) laboratory measurements by Beard et al. (1991) as well as Andsager et al. (1999). More recently, it has been shown that with a fully calibrated 2-D video disdrometer (2DVD; Schönhuber et al., 2008) it is possible to determine shape, orientation and fall velocity of individual hydrometeors falling through its 10 cm by 10 cm sensor area (Thurai and Bringi, 2005; Thurai et al. 2007a; Huang et al. 2008). The instrument has also been used in intercomparison studies with C-band polarimetric radars in various locations such as Okinawa (Bringi et al. 2006), Toronto (Thurai et al., 2007b) and Alabama (Thurai et al. 2009). In the latter, drop-by-drop information (D_{eq}, shape and orientation) from the 2DVD was utilized to compute the individual scattering contributions from which the C-band polarimetric radar parameters such as differential reflectivity (Z_{dr}), specific differential propagation phase (K_{dp}) and the co-polar correlation coefficient (ρ_{co}) were calculated. Comparisons with radar measurements indicated that significant variation in drop shapes can occur at times (i.e. under certain conditions) from the mean or the 'most-probable' shapes.

In this paper, we present another study on drop shape variation, this time utilizing 2DVD as well as the CP2 radar facility located near Brisbane in SE Queensland, Australia. The facility comprises an S-band radar with polarimetric capability as well as an X-band radar for dual-wavelength measurements. The main beams are well-aligned with 3-dB beam width for both frequencies close to 1^o. We describe here a technique developed to make inferences on drop shapes using the X-band specific attenuation (A_x) and the S-band K_{dp}, together with its variation with the S-band Z_{dr}. The technique is applied to CP2 measurements during a squall-line event, and the drop shape inferences are compared with shape measurements from the 2DVD for the same event.

*Corresponding author address: Merhala Thurai, Dept. of Electrical Engineering, Colorado State University, Fort Collins, CO 80523-1373, USA.
Email: merhala@engr.colostate.edu

2. 2DVD MEASUREMENTS

The 2DVD used in this study is a low-profile unit which was installed in November 2008 at a site 16.2 km NE from the CP2 radar site. Soon after installation, the unit underwent precise calibration procedures to ensure accurate drop shape measurements (details of the calibration procedure can be seen in Schönhuber et al., 2008). Since then, several events have been recorded, many of which have been analyzed in terms of shape contours and drop axis ratio distribution for various drop diameter intervals. Fig. 1 shows the contours for (a) 3.0 – 3.25 mm and (b) 4.0 – 4.25 mm drops in probability terms. Superimposed in black are the mean contours given by the set of equations given in Thurai et al. (2007a) derived from the artificial rain (80 m fall) experiment. For the 3 mm contour, there seems very good agreement whereas the 4 mm Brisbane data seems marginally more spherical than the mean shape contour from the 80 m fall experiment (conducted under calm conditions).

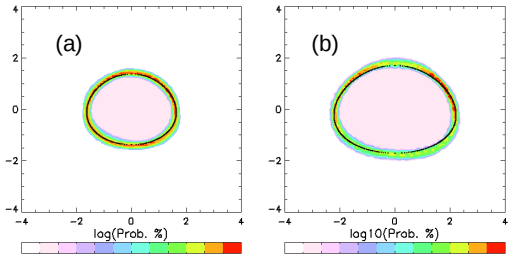

Fig. 1: Shape contours for (a) 3.0-3.25 mm and (b) 4.0 – 4.25 mm drops from the 2DVD measurements in SE Queensland. Superimposed in black are the mean shapes derived from the 80 m fall experiment

In Fig. 2a we show the 2-D histogram (color intensity plot) of the axis ratio distributions versus drop diameter and compare with the variation of the mean and two standard deviations (i.e., ± 2σ) from the 80 m fall experiment (shown in black with error bars). Below 1.5 mm, the 2DVD axis ratio measurements will have decreasing accuracy due to the finite pixel resolution (around 0.2 mm). Above 1.5 mm, there seems generally good agreement; however, note that in the 1.6 – 1.8 mm range, the axis ratios show an unusually

wide distribution, with a significant positive skewness. A similar observation has also been made with 2DVD measurements from other locations such as Huntsville, Alabama. It is likely that this is evidence of oscillations due to the resonance with eddy-shedding frequency, as was observed by Beard et al. (1991) in their laboratory studies (see their Fig. 5 and discussion in their reference). In other diameter ranges, the 2DVD axis ratio measurements show almost the expected distributions.

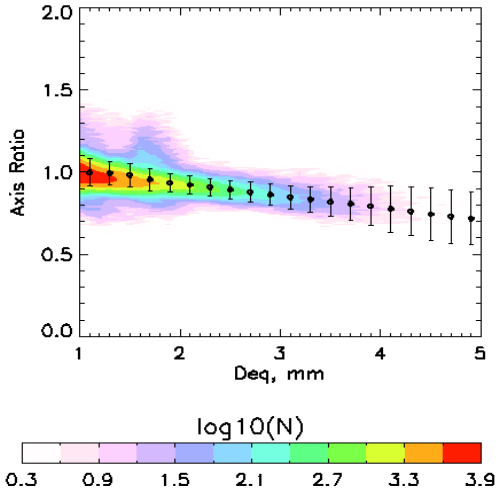

Fig. 2: Axis ratio versus drop diameter (D_{eq}) determined from the 2DVD measurements as color intensity plot, together with the mean and ± 2σ from the axis ratio measurements from the 80 m fall experiment in black.

3. EVENT ANALYSIS

3.1 CP2 Observations

Most of the events recorded by the Brisbane 2DVD in SE Queensland were accompanied by the S-band (dual-polarization) and X band radar observations, with precisely aligned and matched radar-beams. One example was on 19 Feb 2009, a squall-line type event with a leading edge of deep convection, part of which passed over the 2DVD site between 07:40 – 08:00 UTC. The 1-minute drop size distribution (DSD) data from the 2DVD showed the mass-weighted mean diameter (D_m) reaching 2.5 mm at around 07:45.

A low elevation PPI scan taken at 07:43 is shown in Fig. 3, which shows (a) the S-band reflectivity in dBZ for horizontal polarization ($Z_h^{S\text{-band}}$), (b) the X-band measured reflectivity for horizontal polarization ($Z_h^{X\text{-band}}$), (c) the S-band Z_{dr} and (d) the S-band K_{dp} determined from the differential phase measurements. The location of the 2DVD is marked with an asterisk in all cases.

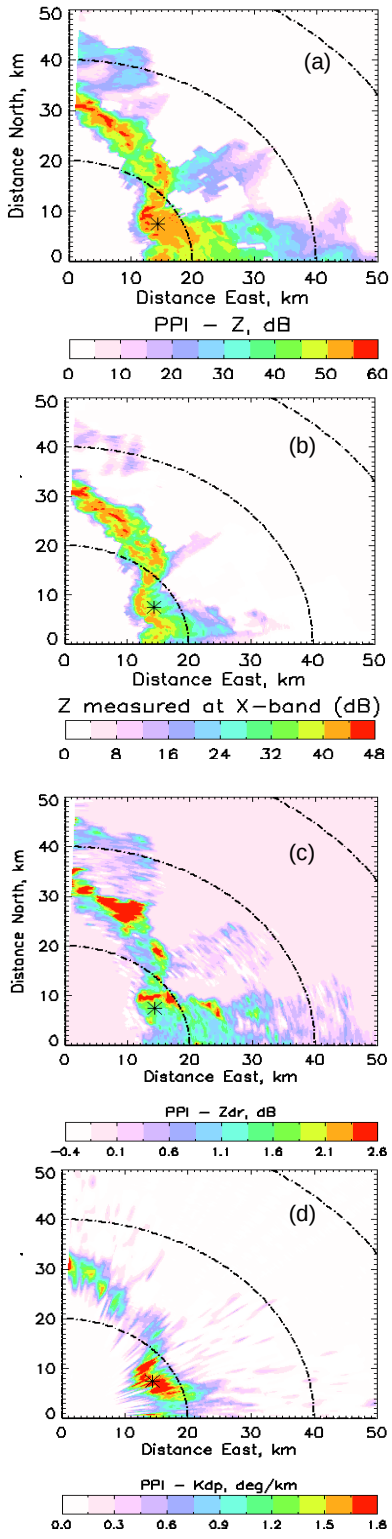

Fig. 3: PPI scan taken at 07:43, (a) $Z_h^{S\text{-band}}$, (b) $Z_h^{X\text{-band}}$, (c) $Z_{dr}^{S\text{-band}}$ and (d) $K_{dp}^{S\text{-band}}$.

The (somewhat unorganized) line of convection is visible in the S-band reflectivity data in Fig. 3(a) as well as in Fig. 3(b) at X-band. The loss of X-band signal beyond the 'squall-line' can also be observed over some azimuth ranges. In the next section, we discuss how to make use of the X-band attenuation along with the S-band polarimetric data for drop shape inferences.

3.2 Utilizing the radar observations

In Appendix A, we consider a simple case where (i) the drop size distribution follow an exponential shape and (ii) the axis ratio varies linearly with drop diameter D_{eq} with a negative slope denoted by β. After certain approximations, it becomes apparent that the ratio r given by $r = A_x / K_{dp}^{S\text{-band}}$ is independent of the DSD but is sensitive to β as well as ζ_{dr} which is the differential reflectivity expressed as a ratio of the H and V polarization reflectivities expressed in units of $mm^6\ m^{-3}$.

To determine A_x we need to ensure that the S band and X band data are matched precisely in azimuth and range. Fig. 4(a: top panel)) shows an example of the range profile taken at 60 deg azimuth, cutting through the high Z_{dr} region (see Fig. 3(b)) just north of the 2DVD site. The narrow range (12-20 km) of the squall-line traversed by the radar beam is evident from the S band reflectivity data in Fig. 4(a). Also evident is the X-band attenuation in the 12-20 km range as well as the complete loss of signal beyond it. The two profiles also imply excellent alignment of both radar beams.

This particular case also had the advantage that there were no rain-on-radome problems which would have affected the X-band measurements. The specific attenuation A_x determined from the two reflectivity profiles is shown in Fig. 4(b: second panel). Superimposed on the same plot are range profiles of the S-band Z_{dr} and the S-band K_{dp}, Note in deriving all three profiles in Fig. 4(b), range filtering was applied using the technique described in Hubbert and Bringi (1995). In Fig. 4(c: third panel) we show the corresponding range profile of the ratio A_x / K_{dp} in units of dB/deg. In the 12 – 20 km range, the ratio is seen to be at around 1. Finally in Fig. 4(d: last panel), we show the ratio r plotted against Z_{dr} for this example range profile: note the ratio is close to unity with a slight increase with range.

Fig. 5 shows (in an enlarged format) the ratio r determined for the whole PPI sector scan in Fig. 3. Apart from the far-side edges of the squall-line (where A_x would be difficult to determine), the values of r seem reasonable, lying in the range 0.5 to 1.5 dB/deg.

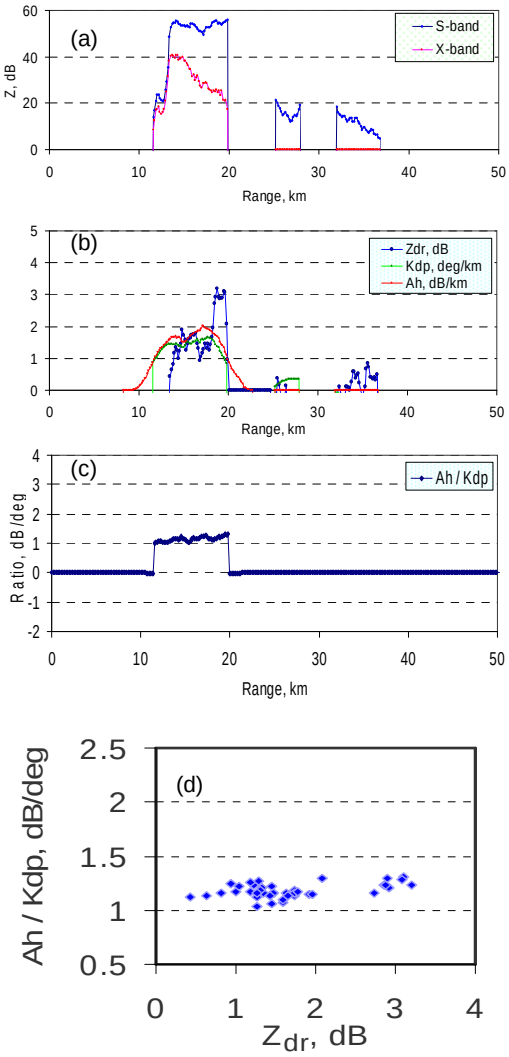

Fig. 4: Range profiles taken at 60 deg azimuth in Fig. 3, of (a) measured S-band and X-band reflectivity, (b) the specific attenuation A_x, the S-band Z_{dr} and the S-band K_{dp}, (c) the ratio r given by A_x/K_{dp} and (d) the variation of r with Z_{dr}.

3.3 Comparing with 2DVD data-based calculations

Although the 2DVD recordings for this event (as in all events) provided drop-by-drop information on shape, size and orientation of each individual hydrometeor (as well as the fall velocity), in our calculations here we have used the 1-minute DSD and bulk assumptions regarding the mean shape and orientation.

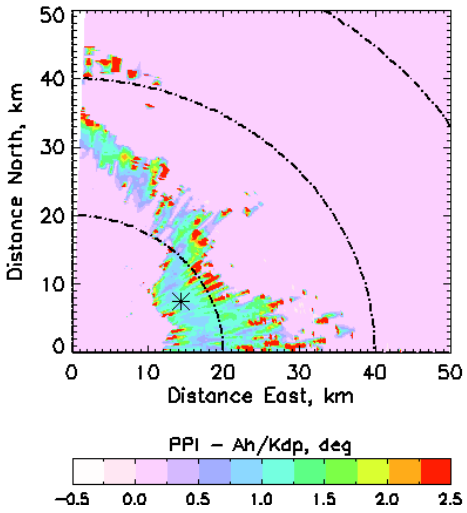

Fig. 5: The ratio *r* determined for the whole PPI sector scan given in Fig. 3.

Fig. 6 compares the CP2 measurements of the ratio versus the S-band Z_{dr} , with 2DVD based calculations. Two cases (top and bottom panels) are considered. In both cases, the CP2 based variations were determined from several PPI sector scans taken during the squall-line event. The color intensity refers to the number of cases with each *r* - Z_{dr} combination from the radar data. Over-plotted on the two identical intensity plots are calculations using the 2DVD 1-minute DSD and (a) using the mean shapes determined from the 2DVD (upper panel) and (b) using the more spherical shapes given in Andsager et al. (1999) (lower panel). Although the CP2 radar based color intensity plot is the same between the top and bottom panels, for clarity, the two sets of 2DVD data based calculations are superimposed in two separate panels. Note in both cases the same 1-minute DSDs from the 2DVD measurements are used, and the same assumptions regarding the canting angle distributions are used (i.e. Gaussian distribution, with 0 deg mean and 7 deg standard deviation). Only the mean shape assumptions used in the 2DVD based calculations are different between Fig. 6(a) and 6(b).

Several points are worth noting from the Fig. 6 comparisons. Firstly, the CP2 radar data-based variation appears much wider than 2DVD-based calculations, mainly due to radar measurement fluctuations; secondly, the calculations using the 2DVD-based mean shapes cut across the most probable variation from the radar data; and thirdly, the 2DVD-based calculations in Fig. 6(b) are displaced above the most probable variation from the CP2 data, but nevertheless, they do lie within the overall variation. Other models for the mean drop shape were not used in our present case study nor did we make use of the drop-by-drop information for the 2DVD data-based calculations for this event. Nevertheless, the above points imply that there are possibly significant shape variations occurring in this event, which tends to corroborate an earlier study (Thurai et al., 2009) conducted in Alabama, using 2DVD drop-by-drop information and concurrent radar observations at C-band.

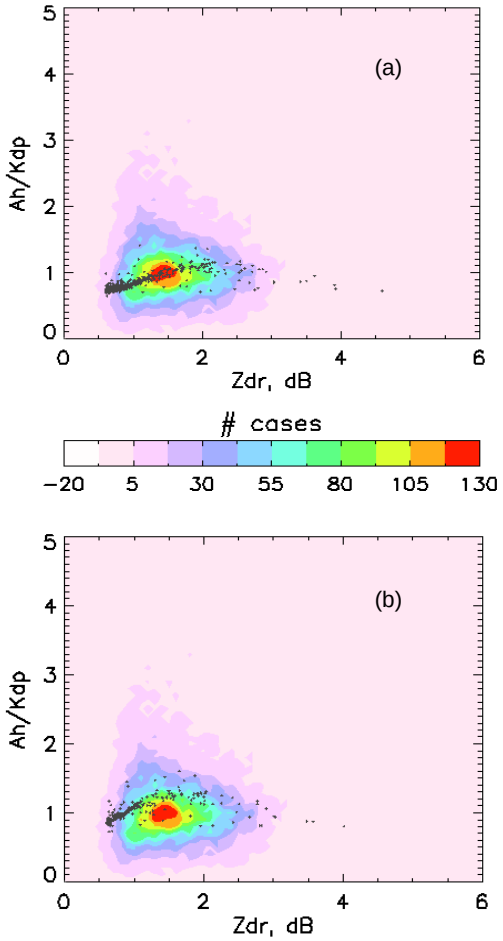

Fig. 6: 2D-histogram in color of the variation of *r* (in dB/deg) with the S-band Z_{dr} determined from several PPI sector scans taken during the same event as Fig. 3, compared with (a: top panel) calculations (shown as black 'dots') using the mean shapes from the 2DVD and the 1-minute DSD and (b: bottom panel) the same calculations but using the Andsager et al. (1999) shapes. In both cases, the same bulk assumptions regarding the canting angle distributions were used. The scatter in the 2DVD-based data can be attributed to changes in the shape of the DSD from minute-to-minute.

4. STEPS TO IMPROVE THE TECHNIQUE

Whilst the 2DVD-based calculations in Fig. 6 can be improved by including the drop-by-drop information, a number of other measures could also be taken to ascertain significant drop shape variations, if any. For example, the CP2 data-based variation in Fig. 6 has contributions due to the 'noisiness' in the S-band Z_{dr} measurements because of poor antenna performance (i.e., poor side lobes and enhanced clutter-to-signal ratio giving lower copolar correlation coefficient in rain and thus higher measurement fluctuations in Z_{dr}). The use of a higher performance antenna would reduce Z_{dr} noise, thus eliminating the need to apply 'heavy' range-filtering. The variation in Fig 6 also has embedded errors due to measurement fluctuations in the dual-wavelength reflectivity ratio and the differential propagation phase (Φ_{dp}) from which A_X and K_{dp} are derived using the iterative range filter described in Hubbert and Bringi (1995). This would give rise to corresponding fluctuations in *r* (even though the S and X band radar beams are well aligned). These errors can be reduced by dwelling the radar beam over the 2DVD site for the duration of the event, rather than rapid PPI sector scans (as was used in this study). The study by Goddard et al. (1982) had clearly demonstrated the usefulness of dwelling over the disdrometer site. Time variation of '*r*' and that of Z_{dr} together with concurrent shape measurements from the 2DVD will greatly help in examining shape variations during various types of events. Performing RHI scans over the disdrometer site at regular intervals will also provide useful information on whether or not significant shape variations occur for deep convective events with high rain rates where collision-induced drop oscillations may occur in a sustained manner. An example of data from an RHI scan taken during the current event is given in Appendix B.

5. SUMMARY AND CONCLUSIONS

The CP2 facility with its precisely aligned S and X band radars provides a good opportunity to conduct observationally-based studies on drop shapes and variations. The well calibrated 2DVD installed 16 km away provides independent measurements of drop shapes (as well as orientations and fall velocities).

Since its installation in November 2008, the 2DVD has recorded several events, many of which have been analyzed to determine the drop shapes and the drop axis ratio distributions for various drop diameter intervals. The modes of the various axis ratio distributions are similar to those from the outdoor, 80 m fall, artificial rain experiment conducted earlier under calm wind conditions. However, in the 1.6-1.8 mm drop diameter range, there seems an unusually wide axis ratio distribution, possibly indicating oscillations due to the resonance with eddy-shedding frequency. 2DVD measurements from other locations such as Alabama, USA and Sumatra, Indonesia, have also shown these unusually wide distributions in the similar diameter interval. Our findings, confirm the laboratory-based measurements of Bead et al. (1991) and their theory of fundamental mode drop oscillations due to resonance with the eddy shedding frequency for the 1.6-1.8 mm sizes.

Most of the events recorded by the 2DVD in SE Queensland were accompanied by the CP2 S-band and X band radar observations, with precisely aligned and matched radar-beams. An analysis technique – independent of radar absolute calibration - has been developed to infer drop shapes from the ratio between the X-band specific attenuation and the specific differential propagation phase at S-band, and its variation with the S-band differential reflectivity. The event analysis has indicated that there could be significant shape variations, but the most probable variation inferred from the radar data agree with the most probable shape measurements from the 2DVD.

Future work will entail refinement of the analysis technique, including the use of drop-by-drop information from the 2DVD, the possible use of higher quality antenna for the S-band radar and the possibility of dwelling along the 2DVD azimuth together with intermittent RHI scans over the disdrometer site. Such improvements will assist in identifying the conditions during which significant shape variations occur. The synergistic approach also provides an insight into drop oscillations and their impact on drop size distribution and rain retrieval algorithms for polarimetric weather radar.

ACKNOWLEDGEMENTS

This work was supported by the US National Science Foundation via grant ATM-0603720. The authors wish to thank Ken Glasson and Michael Whimpey (Centre for Australian Weather and Climate Research) for providing technical support and software assistance respectively, as well as to Dr. Thomas Keenan for his support of this work.

REFERENCES

Andsager K., K.V. Beard, and N.F. Laird, 1999: Laboratory measurements of axis ratios for large raindrops. *J. Atmos. Sci.*, 56, 2673–2683.

Beard K.V., R.J. Kubesh, and H.T. Ochs, 1991: Laboratory measurements of small raindrop distortion. Part I: Axis ratios and fall behavior. *J. Atmos. Sci.*, 48, 698–710.

Beard K. V., and C. Chuang, 1987: A new model for the equilibrium shape of raindrops. *J. Atmos. Sci.*, 44, 1509–1524.

Bringi, V.N., M. Thurai, K. Nakagawa, G. J. Huang, T. Kobayashi, A. Adachi, H. Hanado, and S. Sekizawa,

2006: Rainfall estimation from C-band polarimetric radar in Okinawa, Japan: Comparisons with 2D-video disdrometer and 400 MHz wind profiler, *J. Meteor. Soc. Japan*, 84, 705–724.

Goddard J. W. F., S.M. Cherry, and V.N. Bringi, 1982: Comparison of dual-polarization radar measurements of rain with ground-based disdrometer measurements. *J. Appl. Meteor.*, 21, 252–256.

Gorgucci E., V. Chandrasekar, V. N. Bringi, and G. Scarchilli, 2002: Estimation of raindrop size distribution parameters from polarimetric radar measurements. *J. Atmos. Sci.*, 59, 2373–2384.

Hubbert, J. and V.N. Bringi, 1995: An iterative filtering technique for the analysis of copolar differential phase and dual frequency radar measurements, *J. Atmos. Ocean. Tech.*, 12, 643-648.

Huang G. J., V. N. Bringi, and M. Thurai, 2008: Orientation angle distributions of drops after 80-m fall using a 2D video disdrometer. *J. Atmos. Ocean. Tech.*, 25, 1717–1723.

Jameson A. R., 1983: Microphysical interpretation of multi-parameter radar measurements in rain. Part I: Interpretation of polarization measurements and estimation of raindrop shapes. *J. Atmos. Sci.*, 40, 1792–1802.

Pruppacher H.R., and K.V. Beard, 1970: A wind tunnel investigation of the internal circulation and shape of water drops falling at terminal velocity in air. *Quart. J. Roy. Meteor. Soc.*, 96, 247–256.

Schönhuber M., G. Lammer, and W. L. Randeu, 2008: The 2D video disdrometer. Chapter 1 in 'Precipitation: Advances in Measurement, Estimation and Prediction', S. Michaelides, Ed., Springer, 3–31.

Thurai M., and V. N. Bringi, 2005: Drop axis ratios from 2D video disdrometer. *J. Atmos. Oceanic Technol.*, 22, 966–978.

Thurai, M., G.J. Huang, V.N. Bringi, W. L. Randeu and M. Schönhuber, 2007a: Drop Shapes, Model Comparisons, and Calculations of Polarimetric Radar Parameters in Rain, *J. Atmos. Ocean. Tech.*, 24, (6), 1019-1032.

Thurai M., D. Hudak, V. N. Bringi, G. Lee, and B. Sheppard, 2007b: Cold rain event analysis using 2-D video disdrometer, C-band polarimetric radar, X-band vertically pointing Doppler radar and POSS. Extended Abstracts, 33rd Conf. on Radar Meteorology, Cairns, Australia, *Amer. Meteor. Soc.*, paper 10.7A.

Thurai M., V. N. Bringi, and W. A. Petersen, 2009: Rain microstructure retrievals using 2-D video disdrometer and C-band polarimetric radar. *Adv. Geosci.*, 20, 13–18.

APPENDIX A

The ratio 'r' dependence on drop shapes

In this section, we consider how CP2 measurements of A_x, K_{dp} and Z_{dr} could be utilized to infer drop shapes. If we denote the complex forward scattering vector as $\vec{f}$, then for a given drop size distribution $N(D)$, A_x in can be expressed as:

$$A_X = \frac{2\pi}{k}\int Im\left(\vec{f}\right) N(D)\,dD \qquad (1)$$

At X-band,

$$Im\left(\vec{f}\right) \approx C_A\, D^5 \qquad (2)$$

Also, if we denote the forward scattering amplitudes for H and V polarizations as f_H and f_V , then

$$K_{dp} = \frac{2\pi}{\lambda}\int Re(f_h - f_V)\, N(D)\,dD \qquad (3)$$

λ being the wavelength. If we assume the approximation that drop axis ratio α falls linearly with drop diameter with a slope β (as was considered by Gorgucci et al., 2002, for example), given by

$$\alpha = 1 - \beta D \qquad (4)$$

then,

$$Re(f_h - f_V) \approx D^3 (1-\alpha) = D^3\, \beta D = \beta D^4 \qquad (5)$$

For an exponential DSD, it can be shown that K_{dp} becomes

$$K_{dp} \sim N_0\, \beta D_m^5 \qquad (6)$$

where N_0 is the intercept parameter and D_m is the mass-weighted mean diameter, and similarly, A_X becomes

$$A_X \sim N_0\, D_m^6 \qquad (7)$$

From Jameson (1983), we note that :

$$\zeta_{dr} = (1 - \beta D_Z)^{2.33} \qquad (8)$$

where ζ_{dr} is the power ratio when the H and V polarization reflectivities are expressed in linear units and D_Z is given by:

$$D_Z = \frac{E\left(D^7\right)}{E\left(D^6\right)} = C\, D_m = \frac{1}{\beta}\left(1 - \zeta_{dr}^{-2.33}\right) \qquad (9)$$

In the above, *E()* stands for the expectation over the DSD.

The ratio r = A_x / K_{dp} is given by:

$$r = \frac{A_X}{K_{dp}} \sim \frac{1}{\beta} D_m = \frac{1}{\beta}\frac{1}{\beta}\left(1 - \zeta_{dr}^{-2.33}\right) \qquad (10)$$

$$= \frac{1}{\beta^2}\left(1 - \zeta_{dr}^{-2.33}\right)$$

It can be seen that the functional form in equation (10) is almost independent of DSD but is sensitive to β.

For non-exponential DSD and for cases where eq. (4) doesn't represent the drop axis ratio exactly, the simplified version in eq. (10) cannot be directly applied, but instead rigorous calculations using the complex forward scattering amplitudes computed for individual scatterers (drops) need to be performed. Nevertheless, eq. (10) illustrated the reason for using the variation of '*r*' with Z_{dr} to infer drop shapes used in this study.

APPENDIX B : Example of an RHI scan

The event analysis considered in this paper used primarily PPI scans taken during the squall-line event. In this section, we show that the abovementioned technique can also be applied to RHI scans.

Fig. A1 shows an example RHI scan cutting though the same squall-line event (at a much later time), and over a very different azimuth from that of the 2DVD location. The first panel (a) shows the S-band measured reflectivity. The deep convection reaching heights well above the nominal 0 deg isotherm can be seen at 50 – 60 km range. Reflectivity values of over 60 dBZ could be seen, even above 5 km. The second panel shows the S-band Z_{dr}. Values as high as 3 dB are seen in some regions, indicating the presence of big drops. The third panel shows the S-band K_{dp} and the fourth panel shows A_X determined from the dual frequency ratio between the X-band and the S-band measurements. The column of deep convection can be seen to produce significant attenuation at X-band, with A_X as high as 2 dB/km in some cases.

Fig. A2 shows the ratio 'r' obtained from the S and X band data in Fig. A1. Note that a 'data-quality mask' has been applied in order to identify and neglect regions where contributions from non- hydrometeors are present.

Apart from the edges of the deep convection area, and some regions above the nominal 0 deg isotherm height, the ratio 'r' lies in the expected range of 0.8 to 1.5 for rain. If such columns pass over the 2DVD site, analysis of the corresponding RHI scans would enable the 'effective' drop shapes to be determined at various heights, which in turn could be compared with those measured by the 2DVD at ground level. Such comparisons will indicate the likelihood of collision-induced drop oscillations and their role in determining the development of retrieval algorithms of the DSD parameters and rain rate using the polarimetric variables at various frequencies.

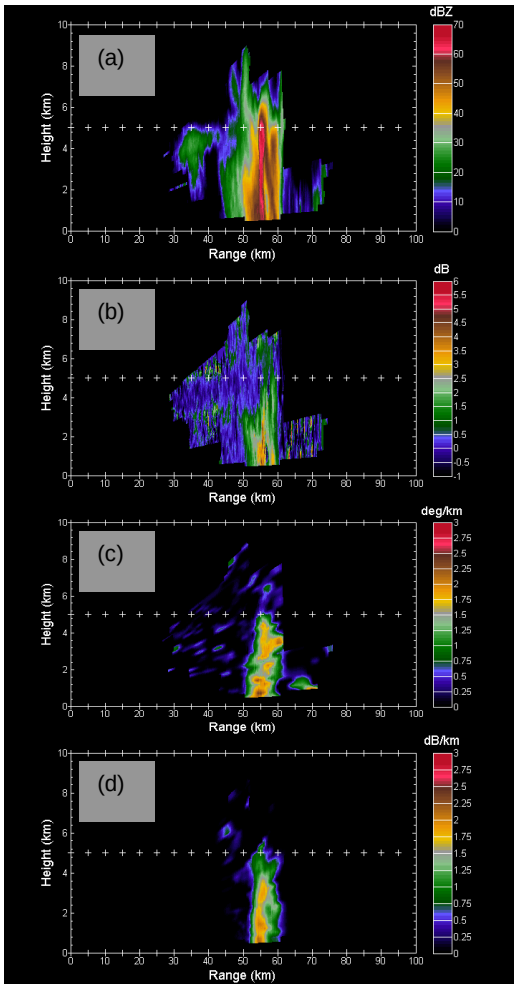

Fig. A1: An example RHI scan cutting through the squall-line; (a) S-band reflectivity, (b) S-band Z_{dr}, (c) S-band K_{dp}, and (d) the ratio '*r*' determined from the dual-frequency ratio measurements at X and S band.

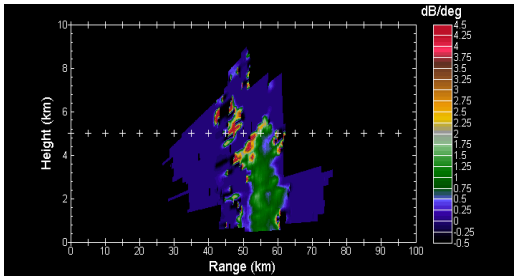

Fig. A2 : The ratio 'r' corresponding to Fig. A1.